Electrical current and coupled electron-nuclear spin dynamics in double quantum dots

G. Giavaras,[1] Neill Lambert,[1] and Franco Nori[1,2]

[1]*Advanced Science Institute, RIKEN, Wako-shi, Saitama 351-0198, Japan*
[2]*Department of Physics, The University of Michigan, Ann Arbor, Michigan 48109-1040, USA*

We examine electronic transport in a spin-blockaded double quantum dot. We show that by tuning the strength of the spin-orbit interaction the current flowing through the double dot exhibits a dip at zero magnetic field or a peak at a magnetic field for which the two-electron energy levels anticross. This behavior is due to the dependence of the singlet-triplet mixing on the field and spin-orbit amplitude. We derive approximate expressions for the current as a function of the amplitudes of the states involved in the transport. We also consider an alternative model that takes into account a finite number of nuclear spins and study the resulting coupled dynamics between electron and nuclear spins. We show that if the spin ensemble is in a thermal state there are regular oscillations in the transient current followed by quasichaotic revivals akin to those seen in a thermal Jaynes-Cummings model.

I. INTRODUCTION

A double quantum dot (DQD) can be used for the detailed investigation of spin interactions among electron spins and even between electron and nuclear spins. The interactions can be probed optically or electrically by monitoring the electrical current flowing through the DQD as a function of the energy offset between the two dots and the applied magnetic field. In a spin-blockaded DQD, the current through the DQD is large when the two electrons form a singlet state, whereas it is suppressed when the two electrons form a triplet state.[1] The spin blockade mechanism is due to the Pauli principle and has been demonstrated in semiconductor heterostructure quantum dots[1] as well as carbon nanotube dots.[2] It has also been shown that the transient behavior of the leakage current can provide valuable information about the interactions between electrons in the DQD and nuclear spins in the host material.[3] In particular, the electrical transport process can lead to a coupled electron-nuclear dynamics, nuclear spin polarization, and hysteresis effects.[1,3,4]

In the spin blockade regime, the small leakage current increases when there is a process that leads to singlet-triplet hybridization (mixing). A non-spin-conserving interdot tunneling is one such process. This type of tunneling may result from a spin-orbit interaction (SOI), which in some cases can be strong enough and thus has to be taken into account.[5,6] The hyperfine interaction (HI) between dot electrons and nuclear spins can also lead to singlet-triplet hybridization. In a simplified approach, the nuclear spins create an effective magnetic field which acts on the electron spins. This field can point in an arbitrary direction and mixes singlet and triplet states.

The electrical current in a DQD system has been examined theoretically in the presence of strong SOI and in the regime where the coupling of the DQD to the leads corresponds to the largest rate in the system.[7] In the first part of this work, we consider a DQD weakly coupled to the leads and examine the current in the resonant regime, i.e., when the lowest singlet and triplet energy levels are almost aligned. Unlike the approach followed in Ref. 7 we consider explicitly the lowest one-electron states and derive rate equations that involve the transition rates between one- and two-electron states. The SOI is modeled with a non-spin-conserving tunnel coupling amplitude t_{so} between the two dots[7,8] which couples the triplet

states $|T_+\rangle$, $|T_-\rangle$ with singlet states. We consider weak SOI, that is $t_{so} < t_c$, where t_c is the spin-conserving interdot tunnel coupling. The effect of a strong SOI on a spin-blockaded DQD has been investigated in Ref. 7 with a more general SOI model in which all triplet states couple to singlet states. Further, we here give emphasis to the regime where the HI is weak enough or absent, which might be the case in carbon-based quantum dots.[9,10] The main aim of the first part of this work is to determine the current as a function of the amplitudes of the one- and two-electron states which participate in the transport cycle. Some approximate results which give valuable insight into the basic behavior of the current are derived. We show that, depending on the strength of the SOI, the current shows a dip at zero magnetic field or a peak when the lowest two-electron energy levels anticross. This behavior occurs because when t_{so} is large the singlet-triplet mixing near zero field is much weaker compared to that at high field. This gives rise to a dip at zero field. However, when t_{so} is small the mixing is strong only near the anticrossing point leading to a peak in the current.

In the second part of this work we focus mostly on the interplay between SOI and HI. To properly account for the HI, we employ a microscopic "toy" model which takes into account a finite number of nuclear spins. To make this model tractable, only the two lowest singlet-triplet states are considered, and we treat the nuclear spins as a single large spin. We first consider the interplay between the SOI and HI, and its effect on the steady state transport and nuclear spin polarization. We find a sharp transition in the current and polarization as the SOI is increased, consistent with the topological phase transition investigated in Ref. 11. Second, we look at the transient dynamics induced by the HI alone, and find a strong oscillatory contribution depending on the hyperfine coupling strength and inversely proportional to the square root of the number of nuclear spins.

II. ELECTRICAL CURRENT IN THE SPIN BLOCKADE REGIME

A. Physical model

In this section the electrical current through the DQD is examined when the electron-nuclear spin dynamics are uncoupled. This section is concerned with the effect of the SOI

on the electrical current while HI-induced effects due to the coupled electron-nuclear dynamics are addressed in the next section. The DQD is modeled with the two-site Hamiltonian

$$H_{\text{DQD}} = H_{\text{c}} + H_{\text{so}} + H_{\text{hf}} + \sum_{i=1}^{2} \varepsilon_i n_i + U \sum_{i=1}^{2} n_{i\uparrow} n_{i\downarrow} + \frac{\Delta}{2} \sum_{i=1}^{2} \sigma_i^z.$$

$$(1)$$

Here H_{c} is the tunnel-coupling Hamiltonian that conserves spin and has the form

$$H_{\text{c}} = -t_{\text{c}}(c_{1\uparrow}^{\dagger} c_{2\uparrow} + c_{1\downarrow}^{\dagger} c_{2\downarrow}) + \text{H.c.},$$

$$(2)$$

and the Hamiltonian part due to the SOI that allows spin-flip has the form[8]

$$H_{\text{so}} = -t_{\text{so}}(c_{1\uparrow}^{\dagger} c_{2\downarrow} - c_{1\downarrow}^{\dagger} c_{2\uparrow}) + \text{H.c.}$$

$$(3)$$

For the HI we assume the form[12]

$$H_{\text{hf}} = +\frac{1}{2} g_{\text{e}} \mu_{\text{B}} (\mathbf{B}_{\text{N},1} \boldsymbol{\sigma}_1 + \mathbf{B}_{\text{N},2} \boldsymbol{\sigma}_2).$$

$$(4)$$

The operator $c_{i\sigma}^{\dagger}$ ($c_{i\sigma}$) creates (destroys) an electron on dot $i = 1,2$ with spin $\sigma = \{\uparrow,\downarrow\}$ and orbital energy ε_i. The number operator is denoted by $n_i = \sum_{\sigma} n_{i\sigma} = c_{i\uparrow}^{\dagger} c_{i\uparrow} + c_{i\downarrow}^{\dagger} c_{i\downarrow}$. The tunnel coupling amplitude between the two dots is t_{c}, the amplitude due to the SOI is t_{so}, the charging energy is U, and $\Delta = g_{\text{e}} \mu_{\text{B}} B$ is the Zeeman splitting due to the external magnetic field B in the z direction. Here $\mathbf{B}_{\text{N},i}$ is the magnetic field in the ith dot due to the nuclear spins and $\boldsymbol{\sigma}_i$ are the Pauli operators.

The quantum states which participate in the transport cycle in the spin blockade regime are the two lowest one-electron states and the five lowest two-electron states. For simplicity the three-electron states are neglected in this study because they do not change qualitatively the basic results. The one-electron eigenstates $|j; n = 1\rangle$ can be written in the general form

$$|j; 1\rangle = \alpha_j |\uparrow, 0\rangle + \beta_j |0, \uparrow\rangle + \gamma_j |\downarrow, 0\rangle + \delta_j |0, \downarrow\rangle,$$

$$(5)$$

with $j = 1,2$ and $c_{1\sigma}^{\dagger} |0\rangle = |\sigma, 0\rangle$, $c_{2\sigma}^{\dagger} |0\rangle = |0, \sigma\rangle$. Here the eigenstates are ordered with increasing energy. In the spin-blockade regime $U \gg t_{\text{c}}$ and further there is an energy offset between the two dots. In this work we choose for the on-site energies $\varepsilon_2 = \varepsilon_1 - U/2$ and define the energy detuning as $\delta = E(1,1) - E(0,2)$, where $E(n,m)$ is the energy of the charge state which has n (m) electrons on dot $i = 1$ ($i = 2$). If $H_{\text{so}} = 0$ and $H_{\text{hf}} = 0$ then $\alpha_1 = \beta_1 = 0$ and $\gamma_2 = \delta_2 = 0$ and the nonzero amplitudes satisfy $\delta_1 \gg \gamma_1$ and $\beta_2 \gg \alpha_2$. When $H_{\text{so}} \neq 0$ the amplitudes α_1, β_1, γ_2, δ_2 are in general nonzero and satisfy $\beta_1 \ll \alpha_1$, $\delta_2 \ll \gamma_2$.

Neglecting double occupation on dot 1, a two-electron eigenstate $|j; n = 2\rangle$ with $j = 3,\dots 7$ has the general form

$$|j; 2\rangle = a_j |\uparrow, \uparrow\rangle + b_j |\uparrow, \downarrow\rangle + c_j |\downarrow, \uparrow\rangle + d_j |\downarrow, \downarrow\rangle$$

$$+ e_j |0, \uparrow\downarrow\rangle.$$

$$(6)$$

Here $|T_-\rangle = |\downarrow, \downarrow\rangle = c_{1\downarrow}^{\dagger} c_{2\downarrow}^{\dagger} |0\rangle$, $|T_+\rangle = |\uparrow, \uparrow\rangle = c_{1\uparrow}^{\dagger} c_{2\uparrow}^{\dagger} |0\rangle$, $|\sigma, \sigma'\rangle = c_{1\sigma}^{\dagger} c_{2\sigma'}^{\dagger} |0\rangle$, and $|S_{02}\rangle = |0, \uparrow\downarrow\rangle = c_{2\uparrow}^{\dagger} c_{2\downarrow}^{\dagger} |0\rangle$. The amplitudes of the various components depend on the strengths of the SOI and HI as well as the Zeeman splitting and detuning.

When $H_{\text{so}} = 0$ and $H_{\text{hf}} = 0$ the two-electron eigenstates correspond to the triplet states $|T_+\rangle, |T_-\rangle, |T_0\rangle = (|\uparrow\downarrow\rangle + |\downarrow\uparrow\rangle)/\sqrt{2}$ and the two singlet states, which consist of the components $|S_{02}\rangle = |0, \uparrow\downarrow\rangle$ and $|S_{11}\rangle = (|\uparrow\downarrow\rangle - |\downarrow\uparrow\rangle)/\sqrt{2}$. The effect of the H_{so} is to couple the $|T_+\rangle, |T_-\rangle$ states to singlet components. As shown below the coupling strength increases with t_{so} and, for a fixed detuning, is sensitive to the Zeeman splitting.

To calculate the electrical current flowing through the DQD we employ a density matrix approach within the Born and Markov approximations.[13] The internal parameters of the DQD and the chemical potentials of the two leads are adjusted to the spin-blockade regime. This regime can be identified from the fact that when $H_{\text{so}} = 0$ and $H_{\text{hf}} = 0$ the three triplet states $|T_+\rangle, |T_-\rangle$, and $|T_0\rangle$ are equally and almost fully populated ($\sim 1/3$), provided spin decoherence is ignored, and the current as a function of the source-drain bias is suppressed.

B. Results

When t_{so} is nonzero the $|T_+\rangle, |T_-\rangle$ states couple to singlet states and this coupling has a direct effect on the current. To demonstrate this effect we show in Fig. 1 the current as a function of the Zeeman splitting Δ and energy detuning δ between the two dots when there is no HI. The coupling of the states is strong near the anticrossing points leading to an increase in the current (see also below). As a result the curves of high current map out the points where the energy levels of the quasi singlet and triplet states anticross. When $t_{\text{so}} = 0$ the leakage current is approximately constant and no high current curves occur.

To understand the role of the SOI we show in Fig. 2 the energy diagram of the two-electron states as well as the current as a function of the Zeeman splitting Δ, for a fixed energy detuning δ and different SOI amplitudes with $H_{\text{hf}} = 0$. We concentrate on the regime $t_{\text{so}} < t_{\text{c}}$ and choose $\delta < 0$, which is experimentally the most interesting case for spin-qubit applications,[1,10,14] because the spin pair can be described by an effective Heisenberg model. The resonant current that is defined as the current at the anticrossing point increases with t_{so}, and the same occurs for the asymptotic current that is defined as the current at a high magnetic field.
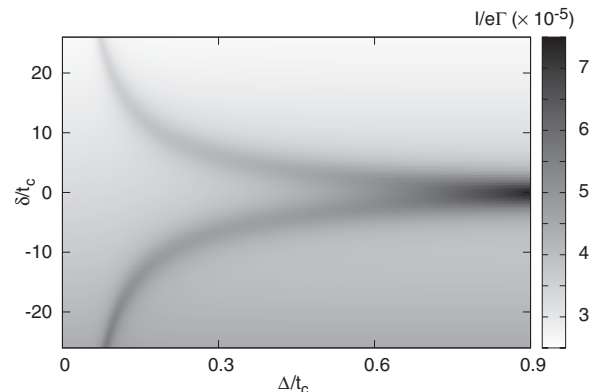

FIG. 1. Electrical current I as a function of the Zeeman splitting Δ and energy detuning δ when there is no hyperfine interaction. The SOI amplitude is $t_{\text{so}} = 0.01 t_{\text{c}}$, where t_{c} is the spin-conserving interdot tunnel coupling.
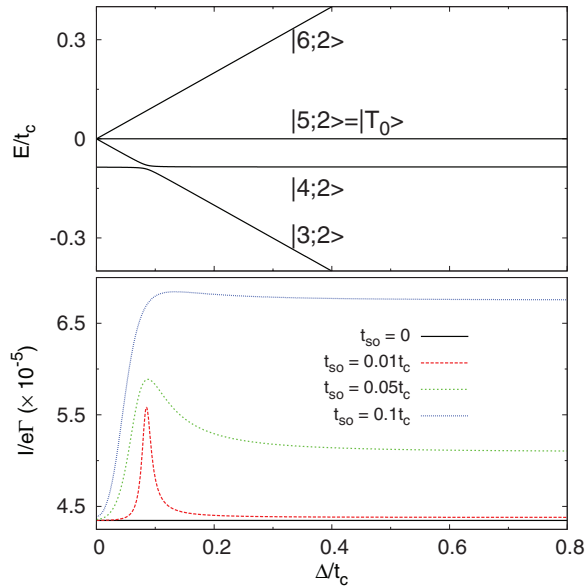
FIG. 2. (Color online) The top panel shows the energies E of the four lowest two-electron states as a function of the Zeeman splitting Δ for an energy detuning $\delta = -25t_c$ and SOI amplitude $t_{so} = 0.1t_c$, where t_c is the spin-conserving interdot tunnel coupling. The notation of the states is given in the main text in Eq. (6). The bottom panel shows the electrical current I as a function of the Zeeman splitting Δ for an energy detuning $\delta = -25t_c$.

Therefore, when t_{so} is large enough the asymptotic current becomes approximately equal to the resonant current and thus the peak cannot be distinguished. The same pattern occurs when the direction of the magnetic field is reversed, thus the current as a function of the Zeeman splitting shows a dip at $\Delta = 0$. To a good approximation this pattern is independent of the detuning, provided t_{so} is large, and consequently the anticrossing points of the energy diagram cannot be probed.

To quantify the above results we analyze the rate equations and calculate analytically the transition rates. Then we derive the steady-state current for some interesting limits, such as for example the current at the singlet-triplet anticrossing point, as well as for $B \sim 0$ and B high. We are interested in determining the current in the steady-state for a DQD that is weakly coupled to the leads. In this regime we can consider only the diagonal elements of the density matrix,[15] and the dynamics of the system is described by the rate equations

$$\frac{d\rho_n}{dt} = -\rho_n \sum_m R_{nm} + \sum_m \rho_m R_{mn}, \qquad (7)$$

where the diagonal elements of the density matrix are denoted by $\rho_n = \rho_{nn}$ and the normalization condition is $\sum_{n=1}^{7} \rho_n = 1$. The transition rate from an eigenstate $|n\rangle$ of the DQD with eigenenergy E_n to an eigenstate $|m\rangle$ with eigenenergy E_m is

$$R_{nm} = \Gamma \sum_\sigma [|\langle n|c_{1\sigma}|m\rangle|^2 f_L(E_{mn}) + |\langle m|c_{1\sigma}|n\rangle|^2 f_L^-(E_{nm})$$
$$+ |\langle n|c_{2\sigma}|m\rangle|^2 f_R(E_{mn}) + |\langle m|c_{2\sigma}|n\rangle|^2 f_R^-(E_{nm})], \qquad (8)$$

where $\Gamma = 2\pi |t_r|^2 D_r/\hbar$. The tunneling amplitude between dot and lead is t_r, $f_\ell(E_{mn})$ is the Fermi-Dirac distribution

function at chemical potential μ_ℓ, with $E_{mn} = E_m - E_n$ and $f^- = 1 - f$. Also, D_r is the density of states for the leads, which we assume to be constant and equal for both leads.

The operator for the electrical current, for example, for the right lead is

$$\hat{I} = \frac{e}{\hbar} i \sum_{k\sigma} t_r(c_{2\sigma}^\dagger d_{k\sigma} - d_{k\sigma}^\dagger c_{2\sigma}), \qquad (9)$$

where $d_{k\sigma}$ denotes a lead operator. Tracing out the leads we derive the following expression for the average current

$$I = e\Gamma \sum_{nm\sigma} \rho_n[|\langle n|c_{2\sigma}|m\rangle|^2 f_R(E_{mn}) - |\langle m|c_{2\sigma}|n\rangle|^2 f_R^-(E_{nm})]. \qquad (10)$$

Starting with the rate equations and calculating the transition rates it can be readily derived that the absolute value of the current for $H_{hf} = 0$ is $I = e\sum_{n=3}^{7}(R_{n1} + R_{n2})\rho_n$. The simplest regime is when $t_{so} = 0$ and $B = 0$. Here, the occupations of the triplet states satisfy $\rho_4 = \rho_5 = \rho_6 = \rho_T$. From the steady-state condition, $d\rho_n/dt = 0$, it can be derived that

$$3\rho_T \approx 1 - \left(\frac{R_{14}}{R_{41} + R_{42}} + \frac{R_{15}}{R_{51} + R_{52}} + \frac{R_{16}}{R_{61} + R_{62}} \right)^{-1}. \qquad (11)$$

For weakly coupled dots the second term is typically negligible and $\rho_T \approx 1/3$. It is easy to prove that this approximation is excellent when t_c is small and δ is large. In this regime the leakage current is

$$I_T \approx 2e\Gamma \left(\frac{R_{14}}{R_{41} + R_{42}} + \frac{R_{15}}{R_{51} + R_{52}} + \frac{R_{16}}{R_{61} + R_{62}} \right)^{-1}. \qquad (12)$$

For $t_{so} \neq 0$ we calculate analytically the transition rates and derive that for low magnetic fields the current is given approximately by the expression

$$I_0 \approx \frac{2e\Gamma}{\frac{1}{2}F_0 + \frac{1}{2}E_0}, \qquad (13)$$

where

$$E_0 = \frac{1}{(\gamma_1 d_4)^2 + (\delta_1 e_4)^2 + (\beta_2 e_4)^2} + \frac{R_{15}}{R_{51} + R_{52}}, \qquad (14)$$

$$F_0 = \frac{1}{(\alpha_2 a_6)^2 + (\alpha_1 a_6 - \delta_1 e_6)^2} + \frac{R_{25}}{R_{51} + R_{52}}. \qquad (15)$$

The transition rates R_{15}, R_{25} involve the one-electron state $|1;1\rangle$, $|2;1\rangle$ respectively, and the triplet state $|T_0\rangle = |5;2\rangle$. The terms which are proportional to R_{12}, R_{25} do not affect the physics we examine here, so for this reason they are not given explicitly. Also, as seen in Fig. 2, in the small t_{so} regime that we are interested in I_0 is to a good approximation independent of t_{so}. An approximate expression for the resonant current is

$$I_r \approx \frac{2e\Gamma}{\frac{2}{3}F_r + \frac{1}{3}E_r}, \qquad (16)$$

with the parameters

$$E_r = \frac{1}{(\gamma_1 d_4)^2 + (\delta_1 e_4)^2 + (\beta_2 e_4)^2} + \frac{R_{15}}{R_{51} + R_{52}}, \quad (17)$$

$$F_r = \frac{1}{(\alpha_2 a_6)^2 + (\beta_2 e_6)^2 + (\alpha_1 a_6 - \delta_1 e_6)^2} + \frac{R_{25}}{R_{51} + R_{52}}. \quad (18)$$

The resonant current corresponds to the magnetic field B_r for which the lowest quasi singlet and triplet states anticross and it is well-defined for $t_{so} \ll t_c$. The asymptotic current that corresponds to a high B is given approximately by the expression

$$I_a \approx \frac{2e\Gamma}{\frac{1}{2}F_a + \frac{1}{2}E_a}, \quad (19)$$

with

$$E_a = \frac{1}{(\gamma_1 d_3)^2 + (\delta_1 e_3)^2 + (\gamma_2 d_3 + \beta_2 e_3)^2} + \frac{R_{15}}{R_{51} + R_{52}}, \quad (20)$$

$$F_a = \frac{1}{(\alpha_2 a_6)^2 + (\beta_2 e_6)^2 + (\alpha_1 a_6 - \delta_1 e_6)^2} + \frac{R_{25}}{R_{51} + R_{52}}. \quad (21)$$

The asymptotic current is defined at a high magnetic field where the current varies slowly with B.

Equation (13) can be used to estimate the width of the current peak that occurs at $\Delta_r = g_e \mu_B B_r$. Specifically, if we denote by $\Delta_r - \Delta_1$ the half width at half maximum of the peak, then Δ_1 satisfies the relation $I_0(\Delta_1) = I_r/2$. In the same way the width of the $\Delta = 0$ minimum can be estimated in the regime $I_a \sim I_r$. If Δ_1 corresponds to half of the width then to a good approximation it has to satisfy the relation $I_0(\Delta_1) = I_a/2$.

The variation of the current as a function of the magnetic field and SOI strength is mainly due to the change of the first terms in E_i and F_i. For example, if $t_{so} \ll t_c$, then as can be seen in Fig. 3 only the quantities $(\gamma_1 d_4)^2$, $(\alpha_2 a_6)^2$, and $(\gamma_1 d_3)^2$ which contribute to E_i and F_i are important. Because these quantities are approximately equal we derive that $E_a \approx E_0$ and $F_a \approx F_0$, thus $I_a \sim I_0$. In the same way, at B_r the corresponding amplitudes in Eqs. (17) and (18) lead to $E_0 > E_r$ and $F_0 > F_r$. Thus, $I_r > I_0$ and a peak is formed at B_r. On the other hand, in the range $t_{so} < t_c$ the quantities $(\delta_1 e_3)^2$, $(\gamma_2 d_3 + \beta_2 e_3)^2$, and $(\beta_2 e_6)^2$, $(\alpha_1 a_6 - \delta_1 e_6)^2$ increase drastically (Fig. 3). As a result, E_a and F_a decrease significantly, whereas E_0 and F_0 do not change a lot. Therefore, for intermediate or large t_{so} the asymptotic current I_a is much larger than the current at very low fields and it approaches the current I_r. Eventually as t_{so} increases the current shows a dip for $\Delta = 0$.

Inspection of the various amplitudes involved in the transition rates demonstrates that the important amplitudes in order to understand the current are the e_4 (or e_3 when B is high) and e_6. These amplitudes express the mixing of the $|T_+\rangle$ and $|T_-\rangle$ states with the $|S_{02}\rangle$ component. These amplitudes are responsible for the behavior of the current when t_{so} is included in the model. As shown in Fig. 4, when t_{so} is not too small the mixing of the $|T_+\rangle$, $|T_-\rangle$ states with the $|S_{02}\rangle$ component
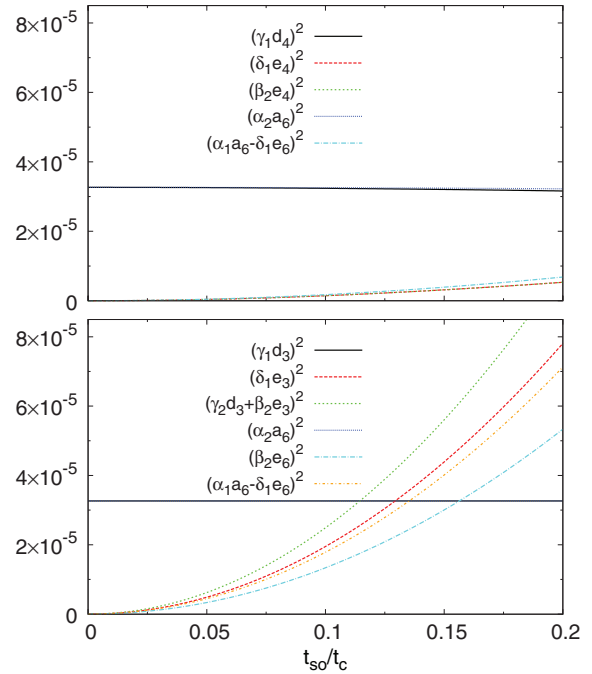

FIG. 3. (Color online) The figure shows the important quantities which determine the transition rates through the parameters F_0, E_0 (top panel), and F_a, E_a (bottom panel) defined in Eqs. (14), (15) and Eqs. (20), (21) respectively. The energy detuning is $\delta = -25t_c$ and the Zeeman splitting is chosen in the low field regime $\Delta = 0.02t_c$ (top) and asymptotic regime $\Delta = 0.7t_c$ (bottom).

is stronger in the asymptotic regime than for $B \sim 0$. For this reason the current is more sensitive to t_{so} when B is high but shows only a small variation with t_{so} for $B \sim 0$. Furthermore, as B increases (in the asymptotic regime) then for a fixed t_{so} and negative detuning the amplitude e_6 for the $|T_+\rangle$ state increases, whereas the amplitude e_3 for the $|T_-\rangle$ state decreases. This behavior can be understood by noticing that the corresponding anticrossing points move along the detuning axis in opposite directions. In Eq. (19), $E_a + F_a$ is to a good approximation constant and the current I_a remains constant as Δ increases.
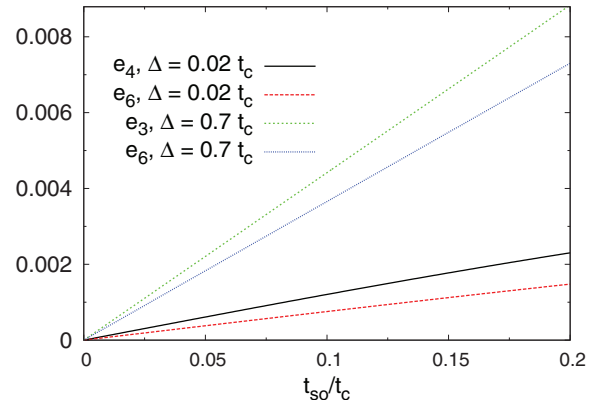

FIG. 4. (Color online) The figure shows the absolute amplitudes e_3, e_4, and e_6 which express the mixing of the triplets $|T_+\rangle$ and $|T_-\rangle$ with the $|S_{02}\rangle$ state. The Zeeman splitting is chosen in the low field regime $\Delta = 0.02t_c$ and asymptotic regime $\Delta = 0.7t_c$.
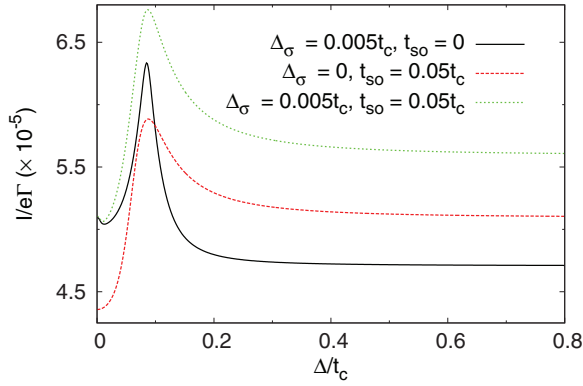
FIG. 5. (Color online) Electrical current I as a function of the Zeeman splitting Δ for the energy detuning $\delta = -25t_c$ and different combinations of SOI and HI strengths. Here $\Delta_\sigma = g_e \mu_B \sigma_N$.

To take into account the hyperfine interaction, we follow a standard approach and treat the nuclear magnetic fields $\mathbf{B}_{N,i}$ in the two dots as quasistatic classical variables which take random values.[12] In this case the electron and nuclear spin dynamics are uncoupled. In the next section we develop a model to look at the coupled dynamics. The distribution for each random static field is Gaussian with spread σ_N. The electrical current is computed as the average over different random field configurations.[12] This is a good approximation when the nuclear dynamics is much slower than the electron dynamics. In Fig. 5 we plot the current versus Zeeman splitting. When $t_{so} = 0$, a peak is formed at the singlet-triplet anticrossing point due to the mixing caused now by the HI. When both t_{so} and σ_N are nonzero the resonant and the asymptotic current increase. However, for $\Delta = 0$ the current is determined by the HI, consistent with the results in Ref. 7. As the spread σ_N increases, the HI results in a peak at $\Delta = 0$, though the $\Delta = 0$ current may have a more complicated form when σ_N is large. In the small σ_N regime that we are interested in and for $t_{so} \neq 0$, the $\Delta = 0$ current is typically smaller than the asymptotic current. Our numerical calculations confirm that these trends occur for different choices of t_{so} provided that $g_e \mu_B \sigma_N \ll t_{so}$.

III. NUCLEAR SPIN POLARIZATION AND TRANSIENT DYNAMICS

A. Physical model

The model employed in the previous section provides insight into the current, but it does not capture the coupled electron-nuclear spin dynamics. Thus, for example, the nuclear spin polarization as a result of the transported electrons through the DQD cannot be examined. In this section we look at the DQD system from a different perspective. Specifically, we use an idealized model to study the coupled electron-nuclear spin dynamics and how this affects the transient behavior of the current. We will use this model to show two things. First, that the presence of even a weak spin-orbit coupling can prevent nuclear spin polarization. Second, if the nuclear spin state is completely thermalized several interesting features arise in the transient electron current; regular beating followed by quasichaotic oscillations.

A true model of the 2^N states which describe the N nuclear spins is computationally intractable, but some insight can be gained from, e.g., treating the nuclear spins as a "giant" spin.[11,16–18] In addition to reduce the complexity even further, we restrict ourselves to a small subspace of the two-electron Hilbert space, spanned by the states $|T_+\rangle$, $|S_{11}\rangle$, and $|S_{02}\rangle$. This is a reasonable approximation under an appropriate bias, i.e., when only the state $|T_+\rangle$ is in the voltage bias window (and neglecting tunneling, from the reservoirs, into superpositions of the singlet states). In addition we assume that the rate of tunneling from the left lead to the dot is large, and that we are at the anticrossing point of the singlet-triplet states.[7] This reduction of the state-space does also neglect the occupation of the $|0,\downarrow\rangle$ state, and trapping in other single-electron-occupation states. As a test, we included the single-electron state $|0,\downarrow\rangle$ in an extended model, but it had little impact on the results we present here. Thus hereafter it will be neglected. In addition, another interesting regime to investigate would be to assume a larger bias and include all three triplet states. However, since all the interesting coupled electron-nuclear effects we discuss here are mediated by the $|T_+\rangle$ and $|S_{11}\rangle$ dynamics, such a regime may only reduce the visibility of these effects.

We model the interaction of these three states with a nonequilibrium master equation. This model allows a flow of electrons through the DQD, and thus we can estimate properties like the total polarization of the nuclear spin, and the transient dynamics of the coupled electron-nuclear spin system. This is in contrast to treating the spins as a frozen spin bath,[19] as a semiclassical degree of freedom,[16,20] or as a non-Markovian environment.[21]

The total Hamiltonian of the system is then written as

$$H = H_c + H_{so} + H_{hf} - \Delta|T_+\rangle\langle T_+| - \delta|S_{02}\rangle\langle S_{02}|, \quad (22)$$

where H_c describes the coupling between the singlet states

$$H_c = t_c[|S_{11}\rangle\langle S_{02}| + |S_{02}\rangle\langle S_{11}|], \quad (23)$$

and H_{so} is the Hamiltonian part due to the SOI, which couples singlet-triplet states, and has the form

$$H_{so} = t_{so}[|T_+\rangle\langle S_{02}| + |S_{02}\rangle\langle T_+|]. \quad (24)$$

The hyperfine interaction is

$$H_{hf} = \frac{g}{2} \sum_{k=1}^{N} \left[|T_+\rangle\langle T_+|I_z^k + \frac{1}{\sqrt{2}} \{\sigma_-^{(1)} I_+^k + \sigma_+^{(1)} I_-^k\} \right]. \quad (25)$$

Here δ is the energy detuning and $\Delta = g_e \mu_B B$ is the Zeeman splitting caused by the external magnetic field B in the z direction, t_{so} is the spin-orbit coupling, and t_c is the coherent tunneling amplitude for the singlets. In H_{hf} we use an effective-spin notation so that $\sigma_+^{(1)} = |T_+\rangle\langle S_{11}|$. The coupling g is the nuclear hyperfine coupling term, $g = A/N$, where N is the number of nuclear spins and A is in the range of 80 μeV.

For simplicity, we assume the nuclear spins are spin-1/2, and the hyperfine coupling strength is uniform and homogeneous. This implies equal-size dots, and an equal nuclear hyperfine coupling on each site. We are working in a rotating frame and the sign difference between couplings on the left and right dots, due to the antisymmetry of the wave function, is omitted.[11] Thus the nuclear states are in fact the

difference between nuclear spin states in the left dot and the right dot. This allows us to use the giant-spin approximation $\hat{J}_i = \sum_k I_i^k, i = z, +, -$. For a large thermal state one should really describe the spin system as a distribution over giant spins of differing sizes.[11] Here we consider a single giant spin of length $J = \sqrt{N/2}$, which may be valid if the distribution of spin sizes is strongly peaked (see Ref. [11] for a rigorous discussion of this assumption). In the final section we discuss the possible effects of a broader distribution.

To account for electron transport we include a Lindblad term,

$$L_1[\rho] = \frac{\Gamma}{2}[2\mu_+\rho\mu_- - \mu_-\mu_+\rho - \rho\mu_-\mu_+], \quad (26)$$

where the electron transport operator is $\mu_- = |S_{02}\rangle\langle T_+|$, and we have omitted the vacuum state which is a good approximation when the rate of tunneling in from the left lead is large. Thus, in the results that we show in the following figures, we solve the master equation for the combined electron-nuclear spin density matrix ρ,

$$\frac{d\rho}{dt} = -\frac{i}{\hbar}[H, \rho] + L_1[\rho]. \quad (27)$$

Because of the small Zeeman splitting of the nuclear spins, we impose an effective infinite temperature for the nuclear system initial state. Nuclear spin dephasing and thermalization are not explicitly included here as they can, in principle, break the large spin approximation, and cannot be written in terms of the J_z operators alone. Fortunately, the nuclear spins are typically weakly interacting with each other and the environment. We assume that the current is dominated by transport into the right reservoir, and is defined as

$$I(t) = e\text{Tr}[\mathcal{J}_\mathcal{R}\rho(t)], \quad (28)$$

where the superoperator is the jump operator $\mathcal{J}_\mathcal{R}[\cdot] = \Gamma\mu_+ \cdot \mu_-$. For the polarization of the nuclear spins we calculate the expectation value of J_z for the large spin.

B. Nuclear spin polarization

Hysteresis in the current measurement, as one sweeps the external magnetic field through the singlet-triplet level crossing, is a sign of nuclear spin polarization. In vertical dots, large polarizations (>40%) have been achieved.[22–25] In lateral dots, the polarizations are significantly smaller, perhaps due to either the asymmetry in the dots, and thus in the nuclear hyperfine interaction, or dark states.[26] However, even for small levels of nuclear spin polarization, large hysteresis has been observed. Further, in several recent studies it has been shown theoretically that if the spin-orbit coupling is above a certain threshold, relative to the nuclear hyperfine coupling, no polarization of the nuclear spin occurs.[11] If it is below that threshold, the nuclear system becomes polarized due to the spin-flip process during the electron transport. At some critical value between these two regimes, long-lived dark states can occur, alongside a topological phase transition.

To investigate this phenomenon in our model we plot, in Fig. 6, both the steady-state current I and the normalized nuclear polarization J_z/J as a function of t_{so} for a given nuclear hyperfine coupling $A = 0.1$ meV. We use dot parameters which put us at the singlet-triplet resonance point, and also

omit the first term (the Overhauser term) in Eq. (25). We see that for

$$t_{so} < 25A/4\sqrt{N}, \quad (29)$$

the nuclear spin is strongly polarized by the electron transport process, and the current flow is low. Conversely, as

$$t_{so} > 25A/4\sqrt{N}, \quad (30)$$

the spin-orbit mediated transport route becomes dominant, and the nuclear spin is no longer maximally polarized. The transition between these two regimes is consistent with the sharp change observed in the "topological phase transition."[11] The factor of 25 arises from the amplitudes $C_{0,2}$ and $C_{1,1}$ of the combined effective singlet state used in that treatment $|S\rangle = C_{0,2}|S(0,2)\rangle + C_{1,1}|S(1,1)\rangle$. Inspection of the bare eigenstates of the electron spin Hamiltonian shows that this factor is, in general,

$$|(C_{1,1}/C_{0,2})| = \left|(\delta - \sqrt{4t_c^2 + \delta^2})/2t_c\right|. \quad (31)$$

Thus the quantum dot system parameters can in practice also be tuned to sweep the axis of Fig. 6. In the bottom half of Fig. 6 we show the absolute value of the matrix elements (in the basis of the $m \in \{-J, J\}$ eigenstates of J_z) of the steady-state nuclear spin density matrix for three choices of spin-orbit coupling: zero, at the "critical point" and far above the critical point. One can easily see that at the critical point there are significant nonzero coherences in the nuclear spin state, which may be related to the presence of long-lived "dark states."[11] Our results indicate that precursors to this "topological phase transition" exist even in the presence of a full transport cycle and noisy environmental effects, akin to the persistence of quantum phase transitions in nonequilibrium systems.[27]

C. Transient dynamics

Some evidence[23,28] indicates that the low dephasing and extremely long relaxation time of the nuclear spins, combined with the fast stochastic electron transport process inducing nuclear polarization, leads to a long time instability phenomenon and fluctuations in the nuclear spin state.[16,20] This is typically observed in the long-time beating seen in the current.[23,28] This is almost certainly a semiclassical effect,[3,16,18,20,29] though some evidence suggests that coherence within the nuclear spins can survive for millisecond time scales.[23] To gain some insight on what might be observed on shorter time scales, we now examine the transient behavior of the electron transport induced by the nuclear spin. In the following we entirely neglect the spin-orbit coupling.

We assume that at some initial time $t = 0$ the electronic system is prepared in the $|T_+\rangle$ state and the nuclear system is in an initially maximally-mixed state

$$\rho(0) = \frac{1}{2J + 1}\sum_m |m\rangle\langle m| \otimes |T_+\rangle\langle T_+|. \quad (32)$$

We then solve the dynamics given by this initial state in the equation of motion. As we will show below, we find that this produces dynamics akin to the Jaynes-Cummings Hamiltonian from quantum optics with an initial thermal (or chaotic) cavity state.[30,31] This is a well-studied system, with
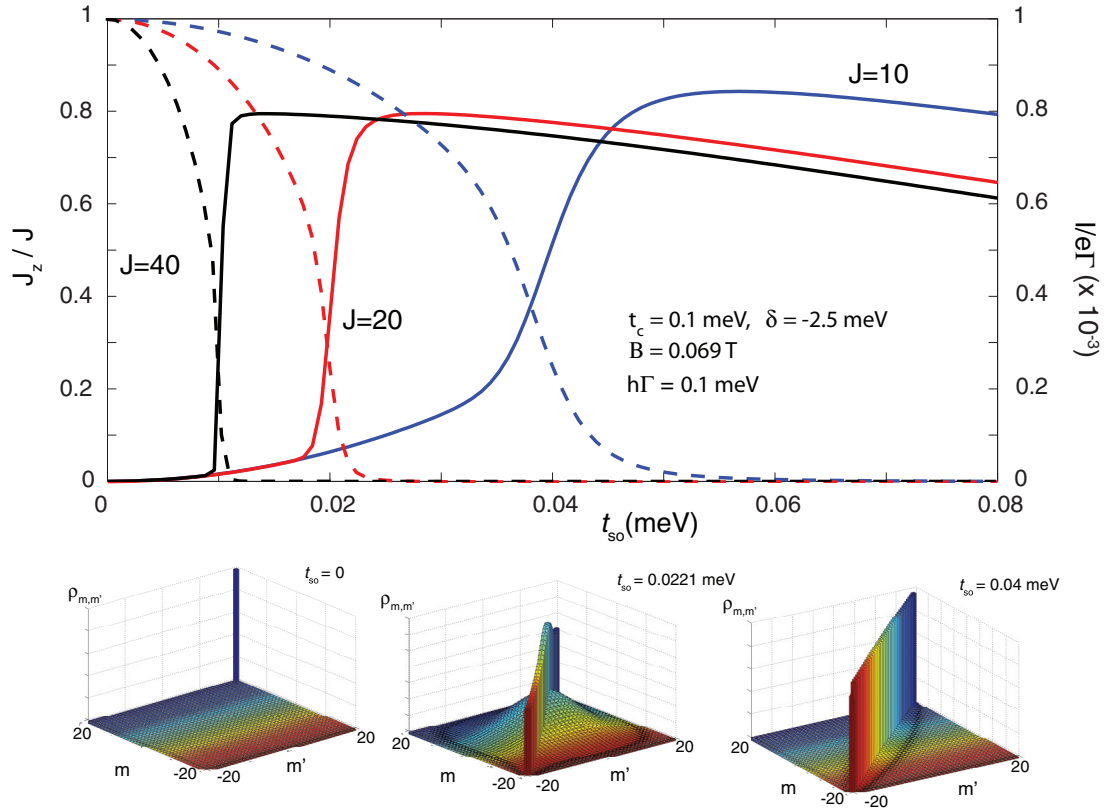
FIG. 6. (Color online) Top: Steady-state current I (solid lines) and nuclear spin polarization J_z (dashed lines) as a function of t_{so}. Three different sizes of large spin are shown, $J = 10$ (blue), $J = 20$ (red), and $J = 40$ (black), corresponding to $N = 200$, 400, and 3800 nuclear spins, respectively. The transition occurs for $t_{so} > 25A/4\sqrt{N}$, where A is the maximum value of the nuclear hyperfine coupling $g = A/N$. Because of the inverse scaling of the transition point, as a function of N, these results suggest that a relatively small spin-orbit coupling can suppress the polarization of the nuclear spin. Bottom: matrix elements (in the m basis of the J_z operator) of the steady-state reduced density matrix of the nuclear spin, for $J = 20$. At the critical point the steady-state contains significant nonzero coherences.

so-called "quasichaotic revivals." In the optical case, studies have shown that one observes an initial sharp peak[31] in the atomic state on a time-scale $t_p^{(bosonic)} \approx 2\pi\hbar/\lambda\sqrt{\bar{n}}$, where λ is the field-atom coupling in that model, and $\bar{n}$ is the initial thermal occupation of the field given by the Bose-Einstein distribution. This is typically followed by the onset of the so-called "quasichaotic" oscillations at a time that scales with the thermal occupation.

In Fig. 7 we show the transient electron current for two sizes of the nuclear spin system. Again we omit the Overhauser term. In the figure, one can see the clear onset of quasichaotic beating and a scaling of the onset of this beating with the size of the large spin J. Since we are now dealing with an infinite-temperature large spin, the role played by $\bar{n}$ in the optical case is now played by J in the large-spin case. Unlike in the optical case, however, the collapse of an initial peak is not seen here. Instead, there is a transition from large steady oscillations to quasichaotic ones.

To understand the presence of the large steady oscillations we can make two observations. Firstly, for low thermal occupation $\bar{n} \ll J$, and large J, the Holstein-Primakoff transformation tells us that the dynamics would coincide with that of the bosonic Jaynes-Cummings model, but with renormalized coupling $\lambda \approx A/2\sqrt{2}N$. As $\bar{n} \propto J$, the analogy

should break down. Secondly, the large regular oscillations can be understood by explicit diagonalization of the H_{hf} Hamiltonian (again omitting the first, Overhauser, term), which gives the following expression for the occupation probability of the $|T_+\rangle$ state, assuming that the initial state is $|\psi(0)\rangle = |T_+\rangle \otimes \sum_{m=-J}^{J} C_m |m\rangle$,

$$|\langle T_+|\psi(0)\rangle|^2 = \sum_{m=-J}^{J} |C_m|^2 \cos^2\left(\frac{E_+ t}{\hbar}\right), \qquad (33)$$

where

$$E_+^{(m)} = \frac{A\sqrt{J(J+1) - m(m+1)}}{2\sqrt{2}N}. \qquad (34)$$

In the bosonic case, this is an infinite sum whose frequencies scale as $\sqrt{n+1}$. One can understand the large regular oscillations that occur in the large spin case by considering the contributions to the sum around $m = 0$. This region contributes a large number of terms to the sum, with similar frequencies $E_+^{(m \approx 0)}/\hbar \approx A/4\hbar\sqrt{N}$, which are commensurate at small times. This gives rise to the frequency of the early-time oscillations in Fig. 7.

The possibility to observe both the early-time oscillations and the quasichaotic oscillations in experiment is intriguing.
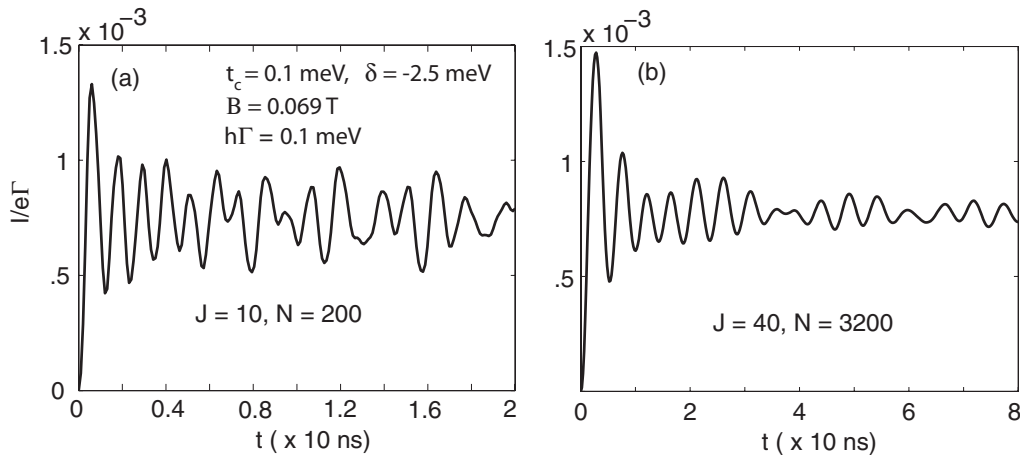
FIG. 7. Transient current $I(t)$ with an initially maximally-mixed nuclear spin state for (a) $J = 10$, and (b) $J = 40$. The large number of commensurate frequencies around $m = 0$ cause the regular oscillations with frequency $A/4\sqrt{N}$, before the onset of quasichaotic dynamics.

One can consider that as N is increased the period of the oscillations increases. For $N \propto 10^5$–10^6 this can reach the order of 100 microseconds. Ultimately, the observation of these oscillations is limited by two effects. First, electron spin dephasing will affect these dynamics. We found that, by including such effects in our model, if these dephasing rates are much larger than the frequency E_+ the oscillations become damped. However, the oscillations are not strongly affected by dephasing or decoherence in the charge degree of freedom. Secondly, in reality, the width of the distribution of large spins in the thermal ensemble around $\sqrt{N/2}$ will also cause dephasing, and is the primary cause of the electron spin dephasing to begin with. One can consider that large spins in this distribution close to $\sqrt{N/2}$ will contribute "in phase" to the early-time oscillations and those far away will induce additional dephasing. Thus, inevitably the oscillations shown in Fig. 7 will decay if this distribution is broad. Finally, dephasing and rethermalization of the nuclear spin states will also affect the dynamics if these rates become comparable to E_+.

In addition, the behavior we show in the dynamics of the current occurs on a relatively short time scale and strongly depends on the initial state. We also emphasize that the meaning of this short-time dynamical current we plot in the figures is the following: it is the ensemble average of detecting the current of a single electron entering the reservoir based on a specific initial condition. In other words, in a real experiment, one would have to repeatedly prepare the nuclear-spin and dot system in the same initial state, and measure the resulting single electron transport events to eventually collate the data shown in the figure. Obviously this is experimentally challenging. A more feasible and natural approach would be to detect transient behavior in the high-frequency current-noise spectrum. However, given that such transients are "around the steady state" (a state which may include significant nuclear spin polarization), some of the features which rely on the nuclear spin state being in a maximally-mixed state may become less visible.

In practice, it maybe more feasible to consider a closed system, i.e., disconnected from electronic reservoirs, and measured by, e.g., a charge detector. In this case there will be no dynamical nuclear polarization, which is advantageous

for observing the features which rely on the maximally mixed state. Also, at this stage, it is not clear if there is any connection between the oscillations we observe here and those seen in experiments. Even for large N the time scales still differ greatly. Finally, an alternative system to investigate this phenomenon could be quantum dots in carbon nanotubes, or with superconducting qubits/wave guides[32] coupled to ensembles of spins in diamond.

IV. CONCLUSIONS

This work investigated electronic transport in a double quantum dot for weak spin-orbit interaction, namely, when the spin-orbit amplitude is smaller than the interdot coupling. The electrical current was calculated numerically from rate equations. We derived simple approximate expressions for the current as a function of the amplitudes of the one- and two-electron states which participate in the transport cycle. We found that when the SOI is small the current shows a peak at a magnetic field for which the lowest two-electron energy levels anticross, whereas when the SOI is large a dip is formed at zero magnetic field. Numerical calculations showed that in a double dot system with a small hyperfine interaction these characteristics remain valid.

We also considered a model which includes dynamical behavior of the nuclear spin, and investigated the coupled dynamics between electron and nuclear spins. We found that the conflict between the spin-orbit and nuclear hyperfine couplings results in a transition point between no polarization and large polarization of the nuclear spin ensemble. We also considered the transient dynamics, where the nuclear spin ensemble is initially prepared in a highly thermal state. The unique characteristics of the large effective-spin model used to describe the nuclear spin ensemble induces dynamics in the current which depends on the fundamental nuclear hyperfine coupling and the ensemble size.

---

[1] K. Ono, D. G. Austing, Y. Tokura, and S. Tarucha, Science **297**, 1313 (2002).

[2] M. R. Buitelaar, J. Fransson, A. L. Cantone, C. G. Smith, D. Anderson, G. A. C. Jones, A. Ardavan, A. N. Khlobystov, A. A. R. Watt, K. Porfyrakis, and G. A. D. Briggs, Phys. Rev. B **77**, 245439 (2008).

[3] K. Ono and S. Tarucha, Phys. Rev. Lett. **92**, 256803 (2004).

[4] R. M. Abolfath, A. Trojnar, B. Roostaei, T. Brabec, and P. Hawrylak, arXiv:1202.5352.

[5] A. Pfund, I. Shorubalko, K. Ensslin, and R. Leturcq, Phys. Rev. B **76**, 161308(R) (2007).

[6] S. Nadj-Perge, S. M. Frolov, J. W. W. van Tilburg, J. Danon, Y. V. Nazarov, R. Algra, E. P. A. M. Bakkers, and L. P. Kouwenhoven, Phys. Rev. B **81**, 201305 (2010).

[7] J. Danon and Y. V. Nazarov, Phys. Rev. B **80**, 041301(R) (2009).

[8] F. Romeo and R. Citro, Phys. Rev. B **80**, 165311 (2009).

[9] A. V. Rozhkov, G. Giavaras, Y. P. Bliokh, V. Freilikher, and F. Nori, Phys. Rep. **503**, 77 (2011).

[10] S. J. Chorley, G. Giavaras, J. Wabnig, G. A. C. Jones, C. G. Smith, G. A. D. Briggs, and M. R. Buitelaar, Phys. Rev. Lett. **106**, 206801 (2011).

[11] M. S. Rudner and L. S. Levitov, Phys. Rev. B **82**, 155418 (2010).

[12] O. N. Jouravlev and Y. V. Nazarov, Phys. Rev. Lett. **96**, 176804 (2006).

[13] C. W. Gardiner and P. Zoller, *Quantum Noise* (Springer, New York, 2000).

[14] J. R. Petta, A. C. Johnson, J. M. Taylor, E. A. Laird, A. Yacoby, M. D. Lukin, C. M. Marcus, M. P. Hanson, and A. C. Gossard, Science **309**, 2180 (2005).

[15] Numerical results derived from the time evolution of the full density matrix confirm that this is a very good approximation, even when degenerate eigenvalues occur, provided the coupling to the leads is weak. We also ignore cotunneling processes.

[16] C. Lopez-Monis, C. Emary, G. Kiesslich, G. Platero, and T. Brandes, Phys. Rev. B **85**, 045301 (2012).

[17] T. Inoshita, K. Ono, and S. Tarucha, J. Phys. Soc. Jpn. Supp. A **72**, 183 (2002).

[18] T. Inoshita and S. Tarucha, Physica E **22**, 422 (2004).

[19] I. A. Merkulov, AI. L. Efros, and M. Rosen, Phys. Rev. B **65**, 205309 (2002).

[20] M. S. Rudner, F. H. L. Koppens, J. A. Folk, L. M. K. Vandersypen, and L. S. Levitov, Phys. Rev. B **84**, 075339 (2011).

[21] W. Yang and R-B. Liu, Phys. Rev. B **78**, 085315 (2008).

[22] J. Baugh, Y. Kitamura, K. Ono, and S. Tarucha, Phys. Rev. Lett. **99**, 096804 (2007).

[23] R. Takahashi, K. Kono, S. Tarucha, and K. Ono, Phys. Rev. Lett. **107**, 026602 (2011).

[24] T. Kobayashi, K. Hitachi, S. Sasaki, and K. Muraki, Phys. Rev. Lett. **107**, 216802 (2011).

[25] J. R. Petta, J. M. Taylor, A. C. Johnson, A. Yacoby, M. D. Lukin, C. M. Marcus, M. P. Hanson, and A. C. Gossard, Phys. Rev. Lett. **100**, 067601 (2008).

[26] M. Gullans, J. J. Krich, J. M. Taylor, H. Bluhm, B. I. Halperin, C. M. Marcus, M. Stopa, A. Yacoby, and M. D. Lukin, Phys. Rev. Lett. **104**, 226807 (2010).

[27] E. G. Dalla Torre, E. Demler, T. Giamarchi, and E. Altman, Nat. Phys. **6**, 806 (2010).

[28] D. J. Reilly, J. M. Taylor, E. A. Laird, J. R. Petta, C. M. Marcus, M. P. Hanson, and A. C. Gossard, Phys. Rev. Lett. **101**, 236803 (2008).

[29] J. Danon, I. T. Vink, F. H. L. Koppens, K. C. Nowack, L. M. K. Vandersypen, and Y. V. Nazarov, Phys. Rev. Lett. **103**, 046601 (2009).

[30] A. B. Klimov and S. M. Chumakov, Phys. Lett. A **264**, 100 (1999).

[31] P. L. Knight and P. M. Radmore, Phys. Lett. A **90**, 342 (1982).

[32] J. Q. You and F. Nori, Nature (London) **474**, 589 (2011).